RSC Advances

This article can be cited before page numbers have been issued, to do this please use: N. Hussain, P. Gogoi, P. Khare and M. R. Das, *RSC Adv.*, 2015, DOI: 10.1039/C5RA22601E.

View Article Online
DOI: 10.1039/C5RA22601E

Nickel nanoparticles supported reduced graphene oxide sheets: A phosphine free, magnetically recoverable and cost effective catalyst for Sonogashira cross-coupling reaction

Najrul Hussain[ac], *Pranjal Gogoi*[bc]*, *Puja Khare*[d] *and Manash R. Das*[ac]*

[a]Materials Science Division, CSIR-North East Institute of Science and Technology, Jorhat-785006, Assam, India.

[b]Medicinal Chemistry Division, CSIR-North East Institute of Science and Technology, Jorhat-785006, Assam, India.

[c]Academy of Scientific and Innovative Research, CSIR, India

[d]Agronomy & Soil Science Division, CSIR-Central Institute of Medicinal and Aromatic Plants, Near Kukrail Picnic Spot, Lucknow-226015, Lucknow India

Abstract

In this study, we have developed a cost effective and one-pot strategy toward the synthesis of heterogeneous catalyst of Ni nanoparticles- reduced graphene oxide composite for Sonogashira cross-coupling reaction. Several characterization tools were employed to characterize the Ni nanoparticle-reduced graphene oxide composites, which indicates that magnetic Ni nanoparticles of the size range of 1-4 nm are uniformly anchored on the reduced graphene oxide nanosheets without using any surfactant or stabilizing agent. Different types of aryl halide and phenyl acetylenes were coupled under optimized reaction condition with excellent yields to give biphenylacetylenes. The ferromagnetic behaviour of the Ni nanoparticle-graphene composite demonstrated the easy separable from the reaction mixture and reusable up to six times without losing its catalytic activity. The fresh as well as reused catalyst in the Sonogashira cross-coupling reaction was well characterized by analytical techniques which show that Ni nanoparticles were well dispersed on the reduced graphene oxide nanosheets without agglomeration and size and morphology of the catalyst remains unchanged after used in the catalytic reaction.

Keywords: Ni nanoparticle, reduced graphene oxide, Sonogashira cross-coupling reaction

*To whom correspondence should be addressed: Manash R. Das (mnshrdas@yahoo.com), Pranjal Gogoi (gogoipranj@yahoo.co.uk)

View Article Online
DOI: 10.1039/C5RA22601E

Introduction

Carbon nanomaterials in catalytic research have received a great attention by the researchers of all over the globe for last two decades. The catalytic performance of the catalyst particularly heterogeneous catalyst is mainly depends on the properties and structure of the support materials. After receiving the Nobel Prize by Andre Geim and Konstantin Novoselov in physics in 2010 for the their ground breaking discovery of 2D material graphene, it is receiving a prime importance as one of the ideal support among all the carbonaceous materials in the heterogeneous catalysts area due to its outstanding properties.[1] Graphene sheets possesses unique 2D crystal structure which easily blended with metals, metal oxides or polymers etc.[1, 2] In recent years, heterogeneous catalyst of metal nanoparticles experienced an enormous progress than homogenous catalyst in terms of stability, selectivity and reusability. In that case metal nanoparticles supported on graphene have attracted significant attention due to its high corrosion resistance, large surface to volume ratio and their excellent dispersive nature. In the last two decades, tremendous efforts have been devoted by the researcher for the development of metal nanoparticle-graphene composite material with controlled size, shape, crystallinity and functionality due to their potential applications in a wide range of fields including supercapacitors,[3] field effect transistors,[4] hydrogen storage,[5] sensors,[6] photocatalysis,[7] soalr cells,[8] molecular imaging,[9] water treatment,[10] catalysis [1, 11] and drug delivery. But in the area of catalysis, metal nanoparticle-graphene composites materials are still to be explored as other applications.[1] The use of metal-graphene composite material as a heterogeneous catalyst has many advantages: a) the graphene as a support prevents the agglomeration and leaching of the metal nanoparticles due to the interaction between the metal atoms and residual oxygen containing functional groups present on the surface of the graphene which results in increase in the surface to volume ratio, b) The presence of 2D structure in graphene results in the superior catalytic performances of

View Article Online
DOI: 10.1039/C5RA22601E

the catalyst because the reactant molecules can absorb to both faces of the catalyst, c) Due to the unique electronic properties of graphene, the electron transfer can take place between the graphene and supported metal nanoparticles which in turn greatly affects the selectivity of the desired product, d) The π-π interaction between the aromatic moieties of reactant molecules and the graphene support enhances the adsorption capacity of the reactant molecules on to the surface of the catalyst.

In view of these advantageous properties of metal-graphene composite materials in heterogenous catalysis, some metal nanoparticles are designed on to the surface of graphene sheets for their catalytic applications such as CO oxidation, oxidation of alcohols, degradation of organic pollutants, hydrogentation of C=C and C=O bond, selective reduction of nitroarenes, fisher-tropsch synthesis and coupling reactions. [1, 13] However, most of these reports deal with the problem of the separation of the catalyst from the reaction mixture which lead to trace amount of metal contaminates on the product. This problem can be easily overcome by designing magnetically separable heterogeneous catalyst. In this regard, the development of environmentally friendly, cost effective, practical, and efficient catalytic processes and its reusability have been attracted worldwide attention in the field of catalysis. Therefore, in this report, we have decorated magnetic Ni nanoparticles onto the surface of reduced graphene oxide sheets (rGO) which shows excellent ferromagnetic properties and thereby results in the effective magnetic separation of the catalyst after completion of the reaction. The magnetic separation of the catalyst is more effective than the filtration or centrifugation as it prevents the loss of the catalyst. Magnetic separation of the catalyst from the reaction system is simple, cost-effective and favorable for industrial applications. The magnetic Ni nanoparticle-rGO composite material is also a low cost heterogeneous catalyst compared to the noble metal (Au, Ag, Pt and Pd) anchored on the graphene sheets.

View Article Online
DOI: 10.1039/C5RA22601E

On the other hand, Sonogashira cross-coupling reaction is one of the most important carbon-carbon bond formation reactions in organic synthesis. This coupling reaction have extensively used for the synthesis of various pharmaceuticals, bioactive compound, natural products, molecular organic materials and engineered materials.[14,15,16] This reaction has developed and admirable results can be obtained with Pd-complexes with phosphine ligands.[17-20] However, the most commonly used phosphine ligands are sensitive to air and moisture, which require inert atmosphere as prerequisite during handling and even a trace amount of such ligand may act as inhibitor in some metal-catalyzed asymmetric reaction.[21] Therefore, the development of ligand-and additive-free Pd catalyst is of immense interest. On the other hand, the use of stable and reusable heterogeneous catalyst to replace the homogenous catalyst for the Sonogashira cross-coupling reaction is of great importance in sustainable chemistry. Various heterogeneous Pd nanoparticles have been developed and efficiently used for the Sonogashira cross-coupling reaction.[22-24] Although some of these catalysts are highly efficient, most of them gave low yield of coupling product even in the presence of different additives.[25-27] To enhance the efficiency of the catalyst, bimetallic nanoparticles comprising Pd metal with other non-noble metals such as copper, nickel, iron and cobalt are used in the Sonogashira cross-coupling reaction. Bimetallic nanoparticles such as Ag–Pd@rGO,[28] Pd/Co alloy NPs,[29] Pd-Co/G alloy NPs,[30] Pd/Cu mixed NPs,[31] Pd/Ni core shell NPs,[32] hollow Pd-Co nanospheres,[33] nano Pd/PdO/Cu system,[34] Pd/Cu nano alloys,[35] rGO-$Cu_{48}Pd_{52}$ alloy nanoparticles [36] are the notable examples which are recently reported for this reaction.

Nickel is promising and cheaper alternative to the use of Pd-based catalyst for the Sonogashira cross-coupling reaction. Among the literature found for the Sonogashira cross-coupling reaction of aryl halides with phenyl acetylenes catalyzed by nickel, Yin *et al.* reported the use of mesoporous silica supported Ni(II) organometallic complex as reusable

View Article Online
DOI: 10.1039/C5RA22601E

catalyst for Sonogashiracross-coupling reaction.[37] Beletskaya *et al.* reported homogenous Ni(II) species as efficient catalyst for Sonogashira cross-coupling reaction.[38] Farjadian *et al.* showed that poly(vinylpyridine)-grafted silica containing Ni nanoparticle is an efficient catalyst for the Sonogashira cross-coupling reaction of aryl halides and phenyl acetylene.[39] Wang *et al.* reported Ni(0) powder catalysis Sonagashira cross-coupling reaction in presence of cuprous iodide and triphenylphosphine .[40] Recently, Ni-Cu system has developed by Bakherad and his co-workers for the Sonogashira cross-coupling reaction of terminal acetylenes with aryl iodides in presence of sodium lauryl sulphate.[41] Most of these previous reports require either the use of phosphine ligand and surfactant or inert atmosphere during the reaction.

As a part of our continuous efforts for the synthesis of metal nanoparticle – graphene composites materials and application in catalytic field,[42-44] herein we have reported the synthesis of magnetically separable Ni nanoparticles on to rGO sheets under ligand free condition and its application in the Sonogashira cross-coupling reaction in presence of cuprous iodide. To the best of our knowledge there is no report on the Sonogashira cross-coupling reaction catalyzed by magnetic Ni nanoparticles anchored on rGO. In view of this we have developed a heterogeneous catalyst of very cheap, magnetically recoverable and reusable Ni nanoparticle-rGO composites for the Sonogashira cross-coupling reaction.

Results and discussion

Characterization of Ni nanoparticles-rGO composites

The formation of Ni nanoparticles on the rGO sheets was confirmed by using analytical tools like X-ray diffraction (XRD), Fourier transform Infrared spectrocscopy (FTIR),

View Article Online
DOI: 10.1039/C5RA22601E

Thermogravimetric analyses (TGA), Transmission Electron Microscope (TEM), Scanning electron microscope- Energy-dispersive X-ray spectroscopy (SEM-EDS) and Vibrating Sample Magnetometer (VSM) analysis. XRD analysis as shown in Fig. 1 revealed that the 2θ values 44.73^{o}, 52.13^{o} and 76.84^{o} corresponding to *d* values 2.02, 1.75 and 1.24 Å are assigned to the well resolved (111), (200) and (220) crystallographic planes of the Ni nanoparticles, respectively. The positions and relative intensities of the diffraction peaks matched well with the standard XRD data of Ni nanoparticle (JCPDS card No. 01-071-4655). It is also confirm that the absence of the NiO and $Ni(OH)_2$ diffraction peak in the XRD pattern of the Ni nanoparticle-rGO composites. It is also noticed that a broad peak at ~25° suggesting that the GO is completely reduced in presence of the hydrazine hydrate.

Thermogravimetric analysis (TGA) as shown in Fig. 2 which provided the information about the reduction of GO to rGO and the formation of Ni nanoparticles onto rGO sheets at the same time. The major weight loss of 37.72% occurred at temperature around 200 ^{o}C is attributed to the decomposition of the labile oxygen-containing functional groups present in GO. The weight loss in this region dramatically decreases upto 9.72% after formation of Ni nanoparticles-rGO composites material because of the reduction of the oxygen containing functional groups present in GO such as carbonyl, hydroxyl, epoxy and carboxyl groups. The weight loss found above 600 ^{o}C for both Ni nanoparticles-rGO composites material and GO are results from the pyrolysis of the carbon skeleton of rGO nanosheets

The catalytic activity of the catalyst mainly depends on the size and shape of the nanoparticles distributed on the support in a heterogeneous catalysis system. In this regards we have examined the morphology of the Ni nanoparticle anchored on the rGO sheets (Fig. 3). The graphene sheets of micron size are clearly visible in the TEM images and Ni

View Article Online
DOI: 10.1039/C5RA22601E

nanoparticles are uniformly distributed onto those sheets. Ni nanoparticles of the mean diameter 2.7 nm with narrow particle size distribution are embedded in the rGO sheets and spherical in nature. The size of our synthesized Ni nanoparticles is very small in comparison to the other previous reports of the synthesis of Ni nanoparticles.[45-49] The small size and uniform distribution of the synthesized Ni nanoparticles is results from the strong interaction between the surface of rGO sheets and Ni nanoparticles.[50] Lu *et. al* proposed that the interaction between the graphene and Ni is attributed to the partially occupied d-orbital which are localized on to the vicinity of the Fermi level.[51] This result clearly fulfils our aim to prepare very small sized nanoparticles and thereby large surface to volume ratio in order to get excellent catalytic activity. Xu *et al.* recently reported the Ni nanoparticle of the average size 9.7 nm decorated on the graphene sheets with narrow size distribution [52]. Wu *et al.* also demonstrated that the synthesis of the Ni nanoparticle-graphene composite by solvothermal method via electrostatic induced spread adsorption. Ni nanoparticle of average size ~55 nm is well distributed on the graphene sheets.[45] Another synthesis method reported by Tian *et al.* observed that Ni nanoparticles of the average size 8 nm homogeneously decorated on the rGO sheets in presence of the poly(N-vinyl-2-pyrolidone) (PVP).[48] However, the Ni nanoparticles of average size of ~27 nm is decorated on the rGO sheets without using stabilizing agent PVP due to agglomeration of the Ni nanoparticles. The surface morphology and elemental composition of the composite material was examined by SEM-EDS (shown in Fig. 4 (a-c)). The crumpled and rippled structure of GO which results from deformation upon the exfoliation is partially destroyed in the composite material due to the reduction of large amount of oxygen containing functional groups (Fig. 4a,b). However, the rGO sheets were layered in structure, it is irregular and folded where the spherical Ni nanoparticles are uniformly distributed. The EDS analysis (shown in Fig. 4c) clearly confirms the sufficient

View Article Online
DOI: 10.1039/C5RA22601E

loading of Ni nanoparticles onto the surface of rGO sheets with an insignificant amount of oxygen which remains due to the presence of unreduced oxygen containing functional group.

The FTIR spectra of GO and Ni nanoparticles-rGO composite is shown in Fig. 5. As shown in Fig. 5, the prominent peaks at 3131, 1728, 1583, 1436, and 1042 cm^{-1} of GO are attributed to the stretching vibrations of O–H, C=O, C=C, C–O–H and C–O–C, respectively. The intensities of these peaks decreased significantly after formation of Ni nanoparticles on rGO sheets due to the reduction of these oxygen containing functional groups present in GO.

To investigate the magnetic properties of our synthesized Ni nanoparticles–rGO composite material, magnetic measurements were performed at room temperature in terms of field dependent magnetization measurement (M-H). The results of saturation magnetization (M_s), remanent magnetization (M_r) and the coercivity (H_c) are listed inside the Fig.6. The hysteresis behaviour and the magnetic parameters clearly reveal the ferromagnetic interaction of the synthesized Ni nanoparticles on rGO nanosheets.[53-56] As shown in Fig. 6, the Ni nanoparticles–rGO composites shows saturation magnetization of 43.54 emu/g and the reduction of this saturation magnetization value in comparison to bulk nanoparticle is due to the increase in surface to volume ratio resulting from decrease in particle size.[54] The Remanence magnetization (Mr) of the sample is found to be 6.92 emu/g and the coercivity (H_c) of 197.54 Oe which is greater than the bulk nickel. The increase in coercivity value in comparison to bulk nickel confirms the rule of $H_C \propto 1/D$ of the multidomain ferromagnetic nanoparticles.[55] Thus, the excellent ferromagnetic behaviour of Ni nanoparticles–rGO composite fulfils our aim to develop more efficient and easily separable catalyst in catalysis reaction.

View Article Online
DOI: 10.1039/C5RA22601E

Catalytic study

After complete characterization of the Ni nanoparticles-rGO catalyst, it was utilized as an effective catalyst for the Sonogashira cross-coupling reaction of aryl halides with phenyl acetylenes in presence of CuI. Initially, we optimized the reaction conditions using bromobenzene **1e** and phenyl acetylene **2a** as model substrates. Different solvents as well as bases were screened and the results are summarized in Table 1. We first examined the effect of solvents on this coupling reaction by using K_2CO_3 as a base. The results revealed that *N*-methyl-2-pyrrolidone (NMP) was the best solvent for this coupling reaction (Table 1, entry 7). Then we examined different bases such as Na_2CO_3, KOH, NaOH and K_3PO_4. The use of strong bases such as NaOH and KOH gave low yield of the product (Table 1, entry 10, 13), whereas Na_2CO_3 and K_3PO_4 showed almost identical results. Additionally, we run the coupling reaction at different temperatures and 120 ^oC was found the optimum reaction temperature for this reaction.

Table 1: Optimization studies for the Ni nanoparticles-rGO catalyst in the Sonogashira cross-coupling reaction [a]

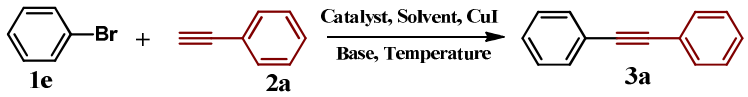

Entry	Solvent	Base	Temperature (^OC)	Yield (%) [b]
1	H_2O	K_2CO_3	110	15
2	DMF	K_2CO_3	60	40
3	DMF	K_2CO_3	120	45
4	Toluene	K_2CO_3	120	30
5	NMP	K_2CO_3	60	70
6	NMP	K_2CO_3	100	85
7	**NMP**	**K_2CO_3**	**120**	**93**
8	DMSO	K_2CO_3	100	80
9	DMSO	K_2CO_3	120	80
10	NMP	KOH	120	50
11	NMP	Na_2CO_3	120	92
12	NMP	K_3PO_4	120	90
13	NMP	NaOH	120	58

[a] Reaction conditions: Bromobenzene (1 mmol), Phenyl acetylene (1.2 mmol), CuI (0.08 mmol), catalyst (25 mg, 0.15 mmol Ni), base (3 mmol), Solvent (5 mL), 4 h. [b] Isolated Yield

View Article Online
DOI: 10.1039/C5RA22601E

After having the optimized reaction conditions, we explored the versatility and efficiency of our catalyst for the Sonogashira cross-coupling reaction using different aryl halides with phenyl acetylenes. The results are shown in Table 2. As shown in Table 2, the aryl halides such as bromides and iodides efficiently coupled with phenyl acetylenes to give the excellent yield of the desired product in spite of electron-rich, electron-poor and electron-neutral nature of the halides. The reaction conditions are notably compatible with nitro group on the aryl ring. Having established a range of aryl bromide and aryl iodide as coupling partner, we next examined the scope of the cross-coupling reaction with aryl chloride (Table 2, entry 14 and 15). Under our optimized conditions, arylchlorides coupled with terminal alkynes and gave good yield of corresponding products. However, the chloroaryl substrate requires long reaction time and high reaction temperature as compared to iodides and bromides in order to get the comparable yield. Additionally our catalyst system chemoselectively reacts with bromide, when both chloro- and bromo- groups were present on the same substrate (Table 2, entry 10). Our catalyst system was also applied to the heteroaryl halide, 2-bromopyridine and the coupling products **3i** were obtained in 86 % yields (Table 2, entries 16). To further extend the scope of our Ni nanoparticles-rGO catalyst in the Sonogashira cross-coupling reaction, we choose a heteroaryl substrate having both bromo and iodo-substituents. In this regard, 2-bromo-5-iodopyridine was treated with three equivalents of phenylacetylene under our catalytic conditions. The product **3j** was obtained with excellent yield (Scheme 1).

Furthermore, we have compared our Ni nanoparticles-rGO catalyst with other previously reported heterogeneous as well as homogenous catalyst of Ni to highlight the advantages of our catalyst in the sonogashira cross-coupling reaction (Table 3). From this comparison results, we have found that our synthesized catalyst is more advantageous with respect to

View Article Online
DOI: 10.1039/C5RA22601E

yield and reaction condition. Moreover, in most of these cases, the scope of their catalyst in Sonogashira cross-coupling reaction is limited to only aryl iodides with phenyl acetylenes.

Table 2: Sonogashira cross-coupling of various aryl halides and phenyl acetylenes [a]

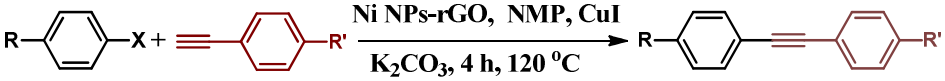

Entry	Aryl halide 1(a-m)	Alkynes 2(a-b)	Product 3(a-i)	Yield [b] (%)
1	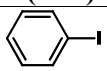 1a	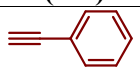 2a	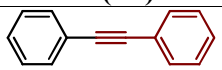 3a	95
2	 1b	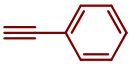 2a	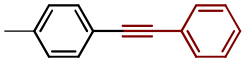 3b	94
3	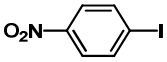 1c	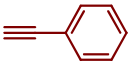 2a	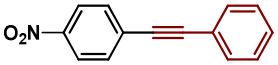 3c	95
4	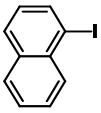 1d	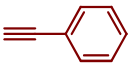 2a	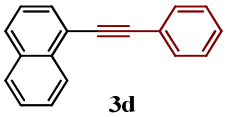 3d	95
5	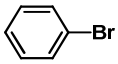 1e	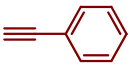 2a	 3a	93
6	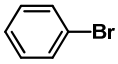 1e	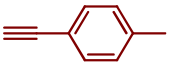 2b	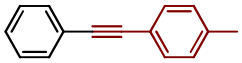 3b	91
7	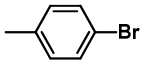 1f	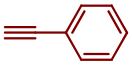 2a	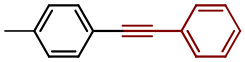 3b	93
8	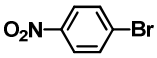 1g	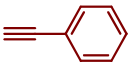 2a	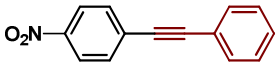 3c	93
9	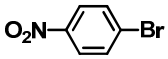 1g	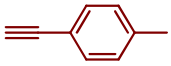 2b	 3e	88
10	 1h	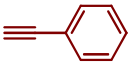 2a	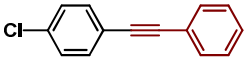 3f	91
11	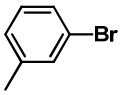 1i	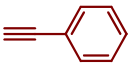 2a	 3g	93

View Article Online
DOI: 10.1039/C5RA22601E

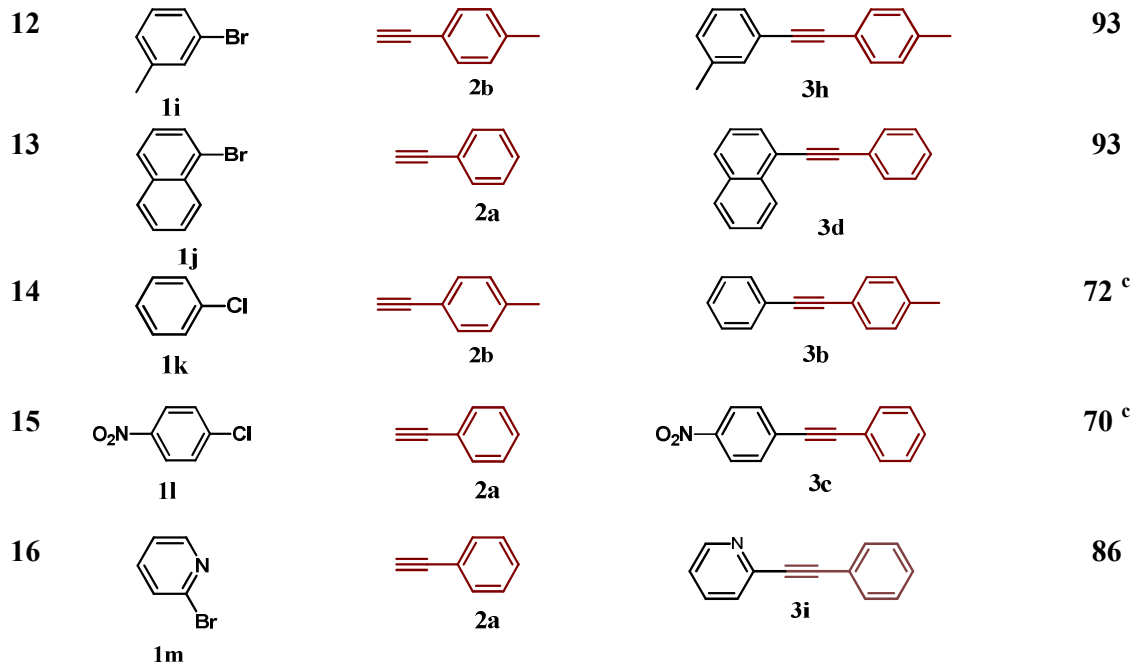

[a] Reaction conditions: Aryl halide (1 mmol), Phenyl acetylene (1.2 mmol), CuI (0.08 mmol), catalyst (25 mg, 0.15 mmol Ni), K_2CO_3 (3 mmol), NMP (5 mL, 120 °C, 4 h. [b] Isolated Yield. [C] The reaction was performed at 140 °C for 16h. NP: nanoparticle

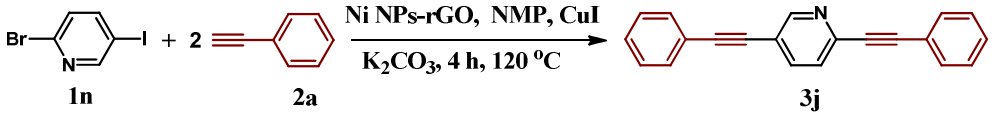

Scheme 1. Ni nanoparticles-rGO catalysed Sonogashira cross-coupling reaction of 2-bromo-5-iodopyridine with phenyl acetylenes.

Table 3: Comparison of catalytic activity of Ni nanoparticles-rGO catalyst with other homogenous and heterogeneous catalyst of Ni

Catalyst	Conditions	Yield (%)	Ref
Ni nanoparticle-rGO	K_2CO_3, NMP, CuI, 120 °C, 4 h	70-95	This work
Si-P4VPy-Ni^0	K_2CO_3, NMP, CuI, 120 °C, 1.5-10 h	40-90	39
$Pd_{70}Ni_{30}$/MWCNTs	NaOH, Pyrrolidine, 120 °C, 1h	60-74	57
$Ni(PPh_3)_2Cl_2$	K_2CO_3, $[Cu(CH_3CN)_4]BF_4$, reflux	57	58
$NiCl_2.6H_2O$- n-Bu_4NBr	NaOH, Ethylene Glycol, 120 °C,1-12 h	46-91	59
$Ni(PPh_3)_2Cl_2$	K_2CO_3, CuI, Dioxane:H_2O, reflux, 4 h	93-100	38
Ni(0)-CuI-PPh_3	KOH, isopropanol, 80-120 °C, 5 h	56-98	40
$Ni(PPh_3)_2Cl_2$/CuI	Cs_2CO_3, H_2O, Surfactant, 60 °C, 2-6 h	70-92	41
Ni-PPh_2-PMOs(Ph)	K_2CO_3, CuI, Dioxane/H_2O, N_2 protection	63-75	37

View Article Online
DOI: 10.1039/C5RA22601E

At present, the exact mechanism of the reaction is not clear. However, we proposed here a plausible mechanism for the Ni nanoparticles-rGO catalyzed Sonogashira cross-coupling reaction as shown in scheme 2. We believed that, the Ni nanoparticles-rGO undergoes oxidative addition with aryl halide to form Ni(II) reactive species which readily transmetalated with Cu-phenylacetylene to form intermediate **A**. Finally the desired coupling product is formed from the resulting intermediate **A** via reductive elimination. [37, 58, 60]

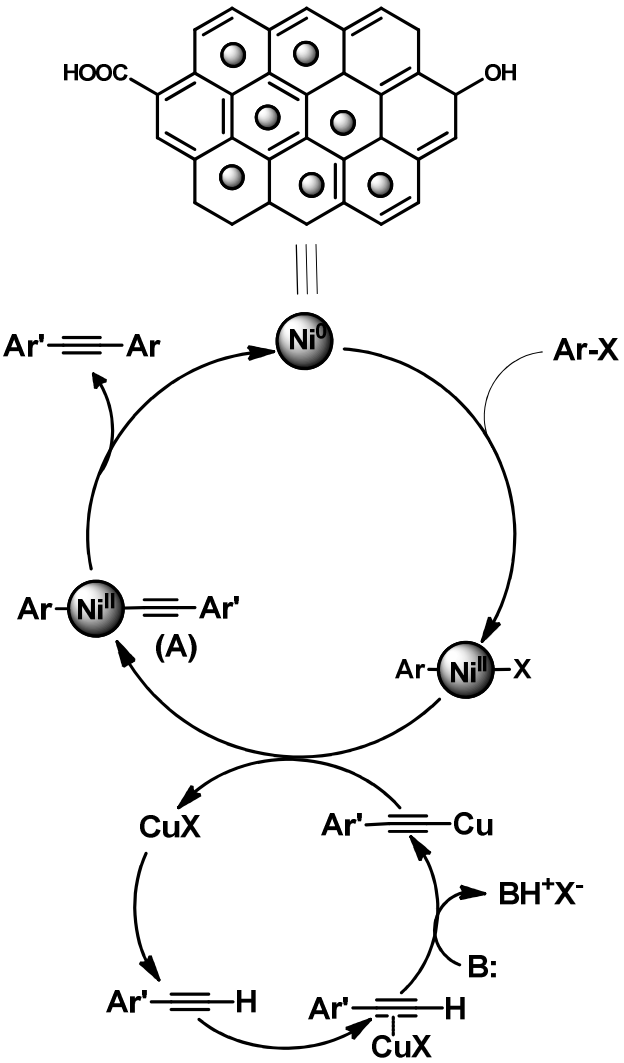

Scheme 2. Proposed mechanism for the Ni nanoparticles-rGO catalyzed Sonogashira cross-coupling reaction

View Article Online
DOI: 10.1039/C5RA22601E

Reusability of the Ni nanoparticle-rGO heterogeneous catalyst

The reusability of our Ni nanoparticles–rGO catalyst for the Sonogashira cross-coupling reaction was also investigated. The excellent magnetic behaviour of our synthesized Ni nanoparticles allows themselves to accumulate onto the magnetic stirring bar as soon as the magnetic stirring was stopped. Therefore, after completion of the reaction, the reaction mixture could be simply and efficiently separated from the catalyst without using any filtration or centrifugation. After separating the catalyst, it was washed with water followed by acetone (2 to 3 times) and dried in an air oven and then directly used for subsequent reaction. To check the reusability of the catalyst, bromobenzene **1e** and phenyl acetylene **2a** was used as substrates for the Sonogashira cross-coupling reaction. As shown in Fig. 7, the recovered catalyst was consecutively used for six times without loss of its significant activity. Although, the different type of heterogeneous catalyst of metal nanoparticles are reported for Sonogashira cross-coupling reaction as discussed in the introduction part, but to the best of our knowledge no reports are available of characterization of the catalyst after performing the reaction. We characterized the Ni nanoparticle-rGO heterogeneous catalyst by XRD and TEM after performing the catalytic reaction as shown in Fig. 8. The average size of the nickel nanoparticles after performing the reaction was found to be ~3 nm which is very close to the 2.7 nm, the average size of the nanoparticles before the reaction. Also we have found the same crystallite size of the Ni nanoparticles for both the fresh and reused catalyst by Sherrer equation using PDXL software in XRD. Therefore, the XRD as well as TEM analysis clearly demonstrate that the size and morphology of the Ni nanoparticle-rGO catalyst remain unchanged after performing the catalytic reaction. Moreover, the nickel content of the recovered catalyst was also determined by ICP-AES which suggest negligible difference with the catalyst before using in organic catalysis reaction.

View Article Online
DOI: 10.1039/C5RA22601E

Since the leaching of the nanoparticles from the support is a common problem in catalysis, we have examined the leaching of Ni nanoparticles from the rGO support by performing hot filtration test. For that we have considered the Sonogashira-cross coupling reaction of bromobnezene **1e** with phenylacetylene **2a**. After continuing the reaction for 1.5 h, the catalyst was separated and the conversion to 1,2-diphenylethyne **3a** was determined by GC and was found to be 45 % yield. After that, the filtrate part was further heated for another 5h to check the progress of the reaction. From the results obtained by GC it was found that no further conversion was observed after separation of the catalyst. This clearly proves that no Ni nanoparticle was leached from the catalyst after performing the reaction.

Conclusion

In conclusion, the present works reports the decoration of very small and uniform sized ferromagnetic Ni nanoparticles onto the surface of rGO sheets. The synthesized composite material shows excellent catalytic activity for the Sonogashira cross-coupling reaction. The catalyst could be easily magnetically separable from the reaction mixture without any leaching of the nanoparticles. The size and morphology of the reused catalyst was again characterized by TEM and XRD which suggest that size and shape of the Ni nanoparticles remain unchanged without undergoing any agglomeration of the particles. In addition, the use of Ni nanoparticle as catalyst for the Sonogashira cross-coupling reaction makes the catalytic process more cost effective. In view of these advantages, the present work represents a new protocol for the synthesis of biphenylacetylenes in an efficient way.

Experimental Section

Materials and Methods

View Article Online
DOI: 10.1039/C5RA22601E

Materials used for synthesis of Ni nanoparticles-rGO composites are graphite powder (<20μm, Sigma-Aldrich), potassium permanganate (>99 %, E-Merck, India), Sulfuric acid (AR grade, Qualigens, India), H_2O_2 (30%, Qualigens, India), hydrochloric acid (AR grade, Qualigens, India), hydrazine Hydrate (80%, LobaChemie, India) and $NiCl_2$ (>97 %, E-Merck, India). All the substrates required for Sonogashira cross-coupling reaction were purchased from sigma Aldrich, USA and used without any further purification.

Characterization techniques

Powder XRD spectra of the samples were taken on a Rigaku, Ultima IV X-ray diffractometer from 5–100° 2θ using Cu-Ka source (l = 1.54 A˚). TGA of the samples were performed at a rate of 5 °C rise in temperature per minute by using TA-SDT (model: Q600DT, TA Instruments, USA). TEM images were taken from JEOL JEM-2011 electron microscope, Transmission Electron Microscope, Japan.VSM, USA operated at room temperature to investigate the magnetic properties of the composite material. SEM-EDS analysis was performed by using Carl ZEISS Field Emission SEM with Oxford EDS to determine the elemental composition of the composite material. FTIR spectra were recorded in the frequency range of400–4000 cm^{-1} on KBr discs in a Perkin–Elmer system 2000 FT-IR spectrophotometer. All NMR spectra were taken by using Bruker Advance DPX 300 or 500 MHz spectrometer. Chemical shifts are reported on the δ scale (ppm) downfield from tetramethylsilane (δ=0.0 ppm) using the residual solvent signal at δ=7.26 ppm (^{1}H) or δ=77 ppm (^{13}C) as internal standard. Gas Chromatography analyses were performed with the help of Chemito GC-8610, FID gas chromatograph fitted with Porapak Q column (2 m × 1/8$^{//}$ O. D., SS) and data were analyzed by Winchrom GC data processing software. Ni content in the nanocomposite catalyst was determined using the EPA 200.7 method of acid digestion followed by Inductively Coupled Plasma Analysis (ICP-AES, Perkin Elmer, Optima 5300 V).

View Article Online
DOI: 10.1039/C5RA22601E

Multilevel Calibration of the Ni was performed using Metal Standard of ICP (Sigma). The calibration curve was linear with R^2 value of 0.99999

Synthesis of Ni nanoparticle-rGO composite materials

$NiCl_2$ (0.338 g) was dissolved in deionised water (10 mL) in a round bottom flask. Then 15 mL of hydrazine hydrate (80%) was mixed with 10 mL of deionised water which was added to the above solution and heated to 75 ^oC for 15 min with stirring. Then 20 mL of an aqueous suspension of GO (0.012 gL^{-1}) was added to above mixture followed by addition of NaOH (20 mg) and subjected to ultrasonication for 10 min. Finally, the reaction mixture was vigorously stirred at 80 ^oC until the black precipitate of the composites material was obtained. The solid material was separated by simple filtration and washed with ethanol for several times followed by water (2 to 3 times) and then dried in an air oven at 60 ^oC for overnight.

General procedure for the Sonogashira cross-coupling reaction

In a round-bottom flask having aryl halide (1 mmol), phenyl acetylene (1.5 mmol), K_2CO_3 (3 mmol) and CuI (0.08 mmol), a suspension of the catalyst (25 mg, 0.15 mmol of Ni) in N-methyl-2-pyrrolidone (5 mL) was added. The whole reaction mixture was stirred at 120 ^oC for 4 h. After completion of the reaction (monitored by TLC), the catalyst was separated from the reaction mixture by using an external magnet and the reaction mixture was poured into water. The organic product was extracted with ethyl acetate (3x10 mL). The combined organic phase were dried over Na_2SO_4 and concentrated in vacuum. The crude products were purified by column chromatography using silica gel (60-120 mesh) with EtOAc/hexanes as eluent to obtain the desired coupling product.

View Article Online
DOI: 10.1039/C5RA22601E

Acknowledgement:

The authors acknowledged the Department of Science and Technology, New Delhi for financial support (DST No. SR/FT/CS-136/2011, CSIR-NEIST Project no. GPP–269 and DST No. INT/RUS/RFBR/P-193 and CSIR-NEIST Project No. GPP-0301) and the Director, CSIR-North East Institute of Science and Technology, Jorhat, India for the interest in this work and facilities. The authors are also thankful to SAIF, NEHU, Shillong for the use of TEM facility. NH acknowledges to UGC, New Delhi, for JRF grant.

References

1. Y. Cheng, Y. Fan, Y. Pei and M. Qiao, *Catal. Sci. Technol.*, 2015, **5**, 3903-3916.
2. V. Singh, D. Joung, L. Zhai, S. Das, S. I. Khondaker and S. Seal, *Prog. Mater. Sci.*, 2011, **56**, 1178-1271.
3. H. L. Wang, H. S. Casalongue, Y. Y. Liang and H. J. Dai, *J. Am. Chem. Soc.*, 2010, **132**, 7472-7477.
4. P. T. Yin, T.-H. Kim, J.-W. Choi and K.-B. Lee, *Phys.Chem.Chem.Phys.*, 2013, **15**, 12785-12799.
5. A. K. Singh, M. A. Ribas and B. Yakobson, *ACS Nano*, 2009, **3**, 1657-1662.
6. J. L. Johnson, A. Behnam, S. J. Pearton and A. Ural, *Adv. Mater.*, 2010, **22**, 4877-4880.
7. Y. Zhang, N. Zhang, Z.-R. Tang and Y.-J. Xu, *J. Phys. Chem. C*, 2014, **118**, 5299-5308.
8. X. Huang, Z. Y. Yin, S. X. Wu, X. Y. Qi, Q. Y. He, Q. C. Zhang, Q. Y. Yan, F. Boey and H. Zhang, *Small*, 2011, **7**, 1876-1902.

View Article Online
DOI: 10.1039/C5RA22601E

9. W. Chen, P. Yi, Y. Zhang, L. Zhang, Z. Deng and Z. Zhang, *ACS Appl. Mater. Interfaces*, 2011, **3**, 4085-4091.
10. R. K. Upadhyay, N. Soin and S. S. Roy, *RSC Adv.,* 2014, **4**, 3823-3851.
11. B. Seger and P. V. Kamat, *J. Phys. Chem. C*, 2009, **113**, 7990-7995.
12. X. Y. Li, X. L. Huang, D. P. Liu, X. Wang, S. Y. Song, L. Zhou and H. J. Zhang, *J. Phys. Chem. C,* 2011, **115**, 21567-21573.
13. X. Huang, X. Qi, F. Boey and H. Zhang, *Chem. Soc. Rev*., 2012, **41**, 666-686.
14. K. Sonogashira, *J. Organomet.Chem*., 2002, **653**, 46-49.
15. S. Atobe, M. Sonoda, Y. Suzuki, H. Shinohara, T. Yamamoto and A. Ogawa, *Chem. Lett.*, 2011, **40**, 925-927.
16. F. Diederich, P.J. Stang, R.R. Tykwinski, Acetylene Chemistry: Chemistry, Biology, and Material Science, Wiley-VCH, Weinheim, 2005.
17. E. Negishi and L. Anastasia, *Chem. Rev.*, 2003, **103**, 1979-2018.
18. R. Chinchilla and C. Najera, *Chem. Rev.*, 2007, **107**, 874-922.
19. R. Chinchilla and C. Najera, *Chem. Soc. Rev*., 2011, **40**, 5084-5121.
20. M. Bakherad, *Appl. Organomet. Chem*., 2013, **27**, 125-140.
21. A. Schumacher, M.G. Schrems and A, Pfaltz. *Chem. Eur. J.*, 2011, **17**, 13502-13509.
22. A. Balanta, C. Godard and C. Claver, *Chem. Soc. Rev*., 2011, **40**, 4973-4985.
23. A. Komaromi and Z. Novak, *Chem. Commun*, 2008, 4968-4970.
24. K. H. Lee, S.-W. Han, K.-Y. Kwon, J. B. Park, *J. of Coll. and Interface Sci.*, 2013, **403**, 127-133.
25. S. Moussa, A.R. Siamaki, B.F. Gupton, M.S. El-Shall, *ACS Catal*., 2012, **2**, 145-154.
26. A. Khalafi-Nezhad, F. Panahi, *Green Chem*., 2011, **13**, 2408-2415.
27. A. S. Singh, S. S. Shendage, J. M. Nagarkar, *Tetrahedron Lett*., 2013, **54**, 6319-6323.

View Article Online
DOI: 10.1039/C5RA22601E

28. M. Chen, Z. Zhang, L. Li, Y. Liu, W. Wang and J. Gao, *RSC Adv.*, 2014, **4**, 30914-30922.
29. S. Ahmad, M. J. Mojtaba, *Mater. Chem. A*, 2013, **1**, 9303-9311.
30. Y.-S. Feng, X.-Y. Lin , J. Hao and H.-J. Xu, *Tetrahedron*, 2014, **70**, 5249-5253.
31. X. Wei, S. Yuanlong, G. Menghan, Z. Weiqiang, G.C. Ziwei, *J. Org. Chem*., 2013, **33**, 820-826.
32. S. U. Son, Y. Jang, J. Park, H.B. Na, H.M. Park, H.J. Yun, J. Lee, T. Hyeon, *J. Am. Chem. Soc.*, 2004, **126**, 5026-5027.
33. H. Li, Z. Zhu, J. Liu, S. Xie and H. Li, *J. Mater. Chem*., 2010, **20**, 4366-4370.
34. M. Korzec, P. Bartczak, A. Niemczyk, J. Szade, M. Kapkowski, P. Zenderowska, K. Balin, J. Lelatko and J. Polanski, *J. Catal.*, 2014, **313**, 1-8.
35. W. Xu, H. Sun, B. Yu, G. Zhang, W. Zhang and Z. Gao, *ACS Appl. Mater. Interfaces*, 2014, **6**, 20261-20268.
36. S. Diyarbakir, H. Can, and O. Metin, *ACS Appl. Mater. Interfaces*, 2015, **7**, 3199-3206.
37. J. Yin, W.Chai, F. Zhang and H. Li, *Appl. Organometal. Chem.*, 2013, **27**, 512-518.
38. I. P. Beletskaya, G. V. Latyshev, A. V. Tsvetkov and N. V. Lukashev, *Tetrahedron Lett*., 2003, **44**, 5011- 5013.
39. F. Farjadian and B. Tamami, *ChemPlusChem*, 2014, **79**, 1767- 1773.
40. L. Wang, P.Li and Y. Zhang, *Chem. Commun*., 2004, 514-515.
41. M. Bakherad, A. Keivanloo and S. Mihanparast, *Synth. Commun*. 2009, **40**,179-185.
42. N. Hussain, P. Gogoi, V. K. Azhaganand, M. V. Shelke and M. R. Das, *Catal. Sci. Technol.*, 2015, **5**, 1251-1260.
43. N. Hussain, A. Borah, G. Darabdhara, P. Gogoi, V. K. Azhagan, M. V. Shelke and M. R. Das, *New J.Chem*., 2015, **39**, 6631-6641.

View Article Online
DOI: 10.1039/C5RA22601E

44. P. Sharma , G. Darabdhara, T. M. Reddy, A. Borah, P. Bezboruah , P.Gogoi , N. Hussain, P. Sengupta and M.R. Das, *Cat. Comm*., 2013, **40**, 139-144.

45. Y. Wu, M. Wen, Q.-S. Wu and H. Fang, *J. Phys. Chem. C*, 2014, **118**, 6307-6313.

46. G. Chen, F. Wang, F. Liu, X. Zhang, *App. Surf. Sci*., 2014, **316**, 568-574.

47. B. Wang, S. Li, J. Liu and M. Yu, *Mat. Res. Bull*., 2014, **49**, 521-524.

48. Y. Tian, Y. Liu, F. Pang, F. Wang and X. Zhang, *Coll. and Surf.s A: Physicochem. Eng. Asp.*, 2015, **464**, 96-103.

49. Z. Liu,Y. Guo and C. Dong, *Talanta*, 2015, **137**. 87-93.

50. M. Zhang, Z. Yan, Q. Sun, J. Xie and J. Jing, *New J. Chem*., 2012, **36**, 2533–2540.

51. Y. H. Lu, M. Zhou, C. Zhang and Y. P. Feng, *J. Phys. Chem. C*, 2009, **113**, 20156-20160.

52. J. Xu, Y. Li, J. Cao, R. Meng, W. Wanga and Z. Chen, *Catal. Sci. Technol*., 2015, **5**, 1821-1828.

53. H. Wang, X. Jiao and D. Chen, *J. Phys. Chem. C*, 2008, **112**, 18793-18797.

54. A. S. Lanje, S. J. Sharma and R. B. Pode, *Archives of Phys. Res.*, 2010, 1, 49-56.

55. X. He, W. Zhong, C.-T. Au and Y. Du, *Nanoscale Res. Lett.*, 2013, **8**, 446.

56. H. Yang, Y. Zhu, P. Sun, H. Yan, L. Lu, S. Wang and J. Mao, *J. Chem. Res*., 2012, **36**, 437-440.

57. A. Ohtaka, J. M. Sansano, C. Najera, I. M.-Garcia, Angel B.-Murcia and D. C. Amoros, *ChemCatChem,* 2015, **7**, 1841-1847.

58. A. Petuker, C. Merten and U.-P. Apfel, *Eur. J. Inorg. Chem*., 2015, **2015**, 2139-2144.

59. N. Nowrouzi, M. Zarei, *Tetrahedron*, 2015, **71**, 7847-7852.

60. V. Polshettiwara, C. Lenb, A. Fihri, *Coord. Chem. Rev.*, 2009, **253**, 2599-2626.

View Article Online
DOI: 10.1039/C5RA22601E

Figures

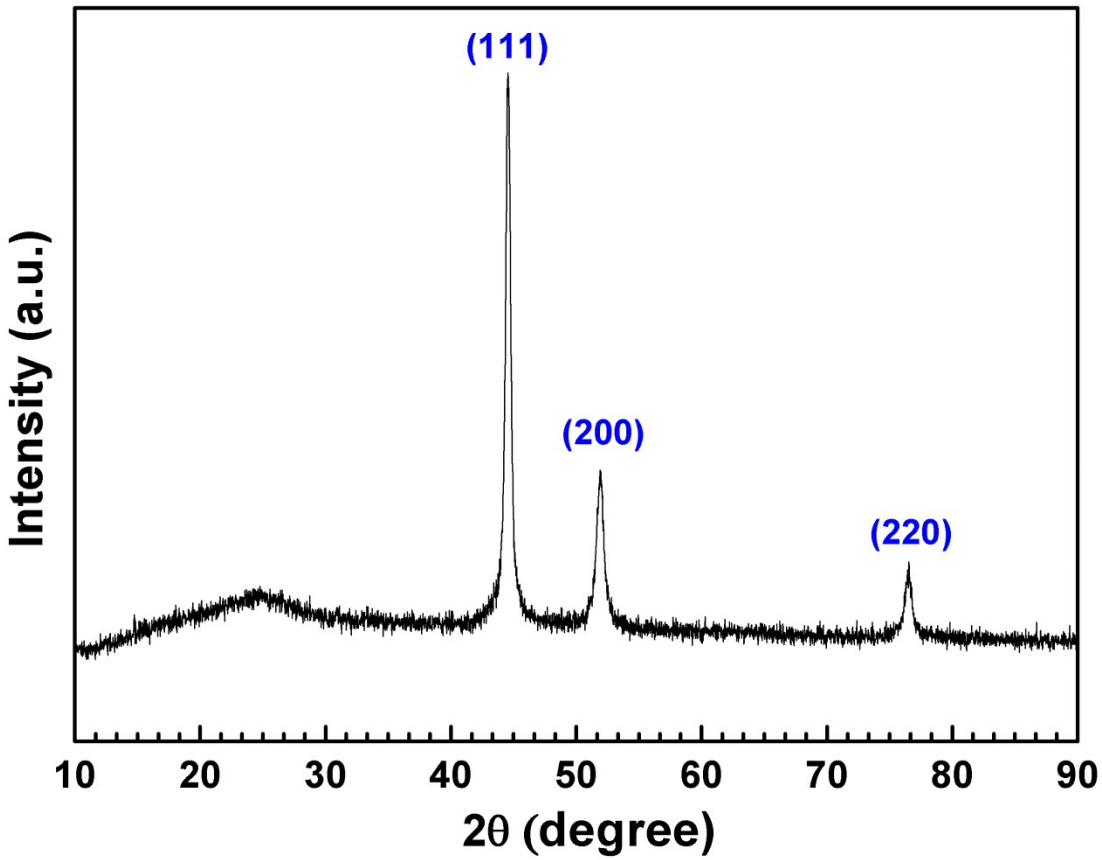

Fig. 1 Powder XRD diffractogram of Ni nanoparticles-rGO composites

View Article Online
DOI: 10.1039/C5RA22601E

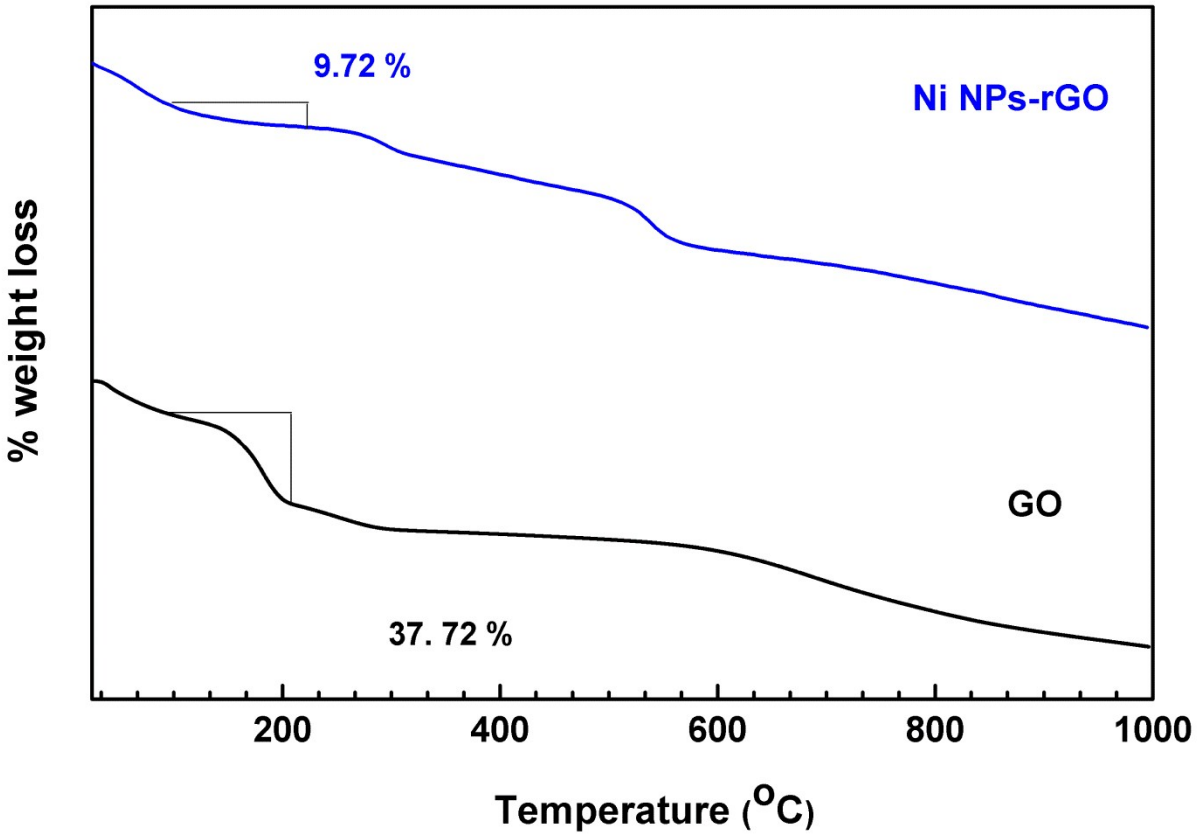

Fig. 2 TGA curve of (a) GO and (b) Ni nanoparticles -rGO composites

View Article Online
DOI: 10.1039/C5RA22601E

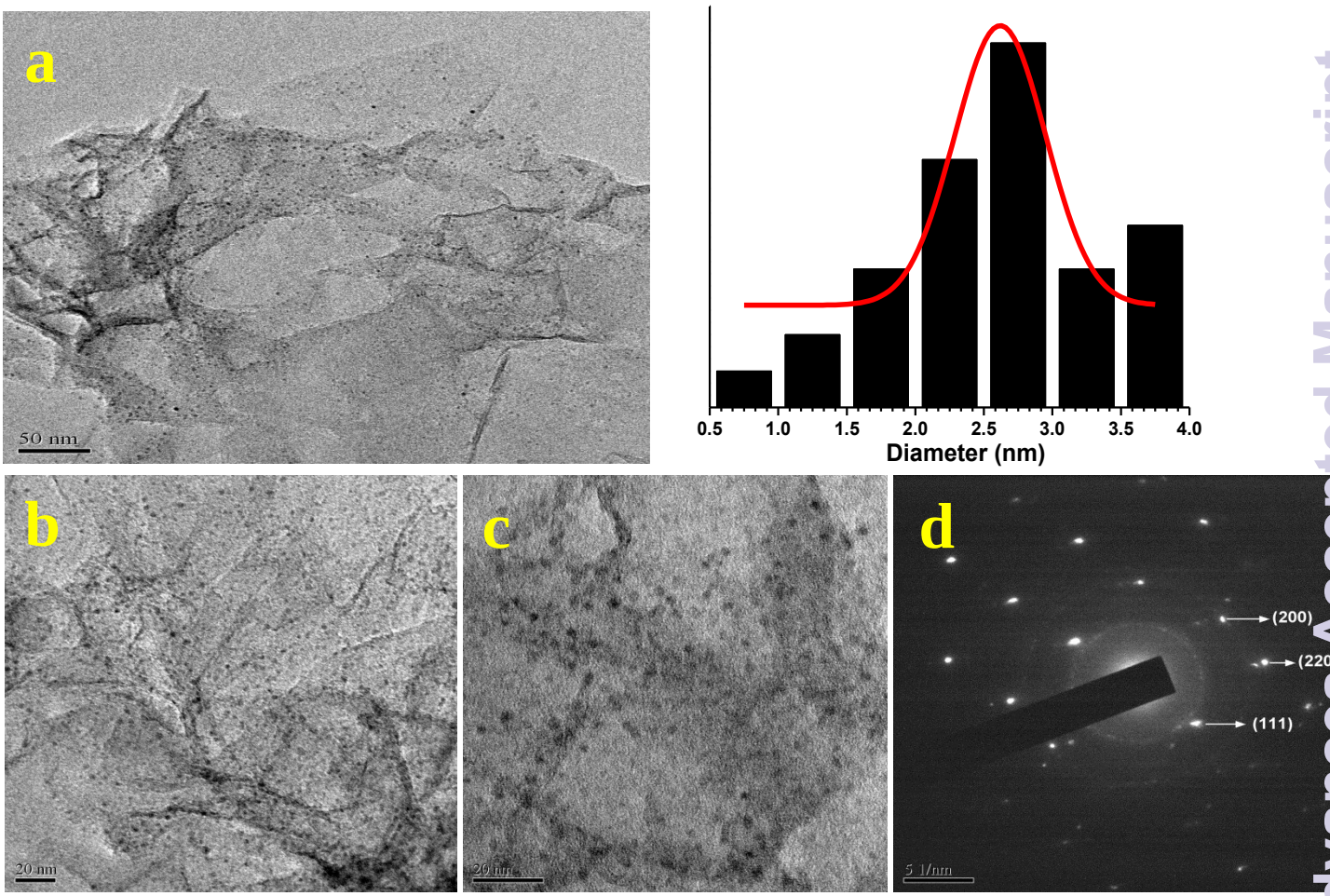

Fig. 3 TEM images of Ni nanoparticle on rGO nanosheets (a-d). HRTEM image along with particle size distribution (a)

View Article Online
DOI: 10.1039/C5RA22601E

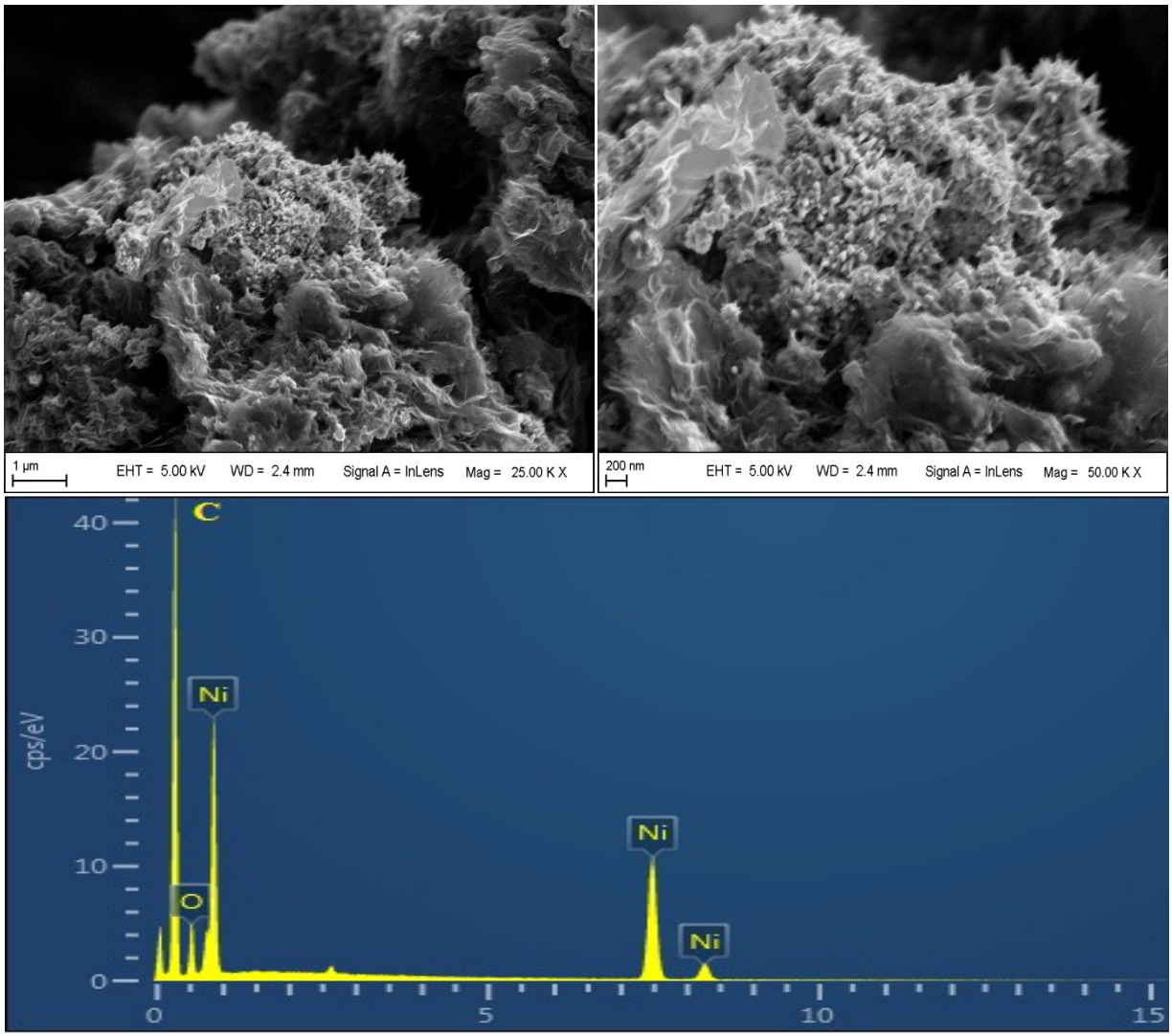

Fig. 4 SEM images of Ni nanoparticles on rGO nanosheets (a-b); EDS analysis of Ni nanoparticles-rGO composite material

View Article Online
DOI: 10.1039/C5RA22601E

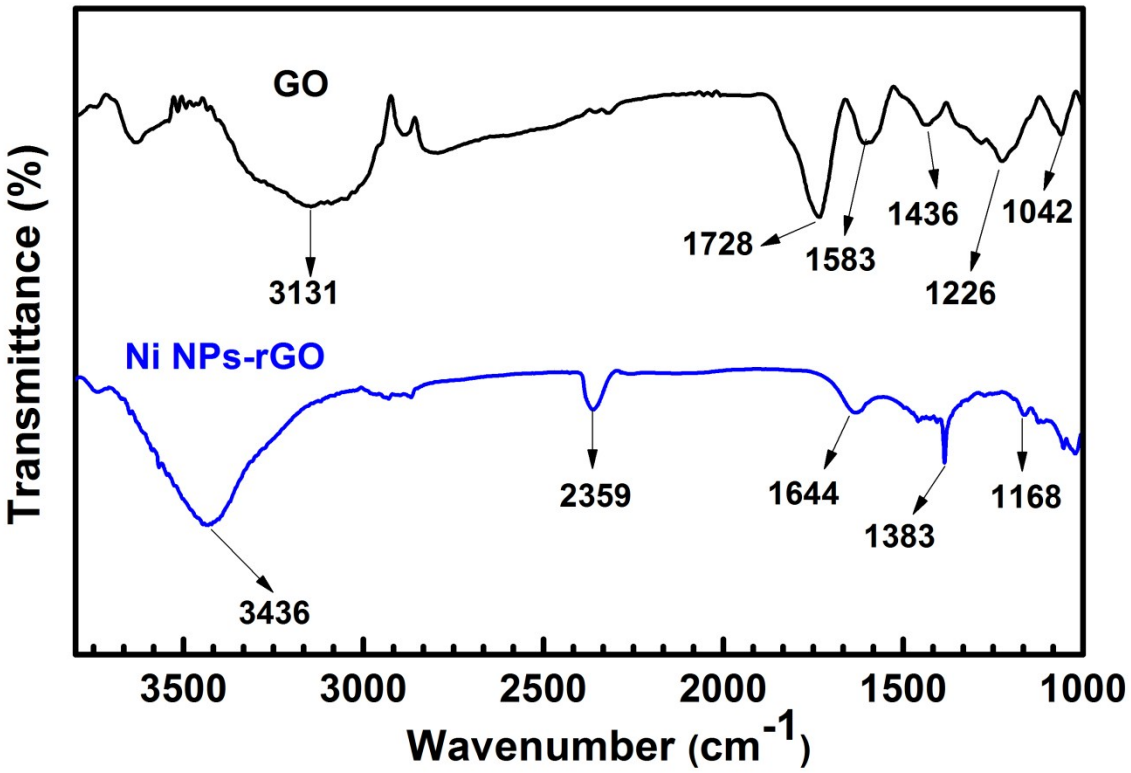

Fig. 5 FTIR spectra of (a) GO and (b) Ni nanoparticles -rGO composite

View Article Online
DOI: 10.1039/C5RA22601E

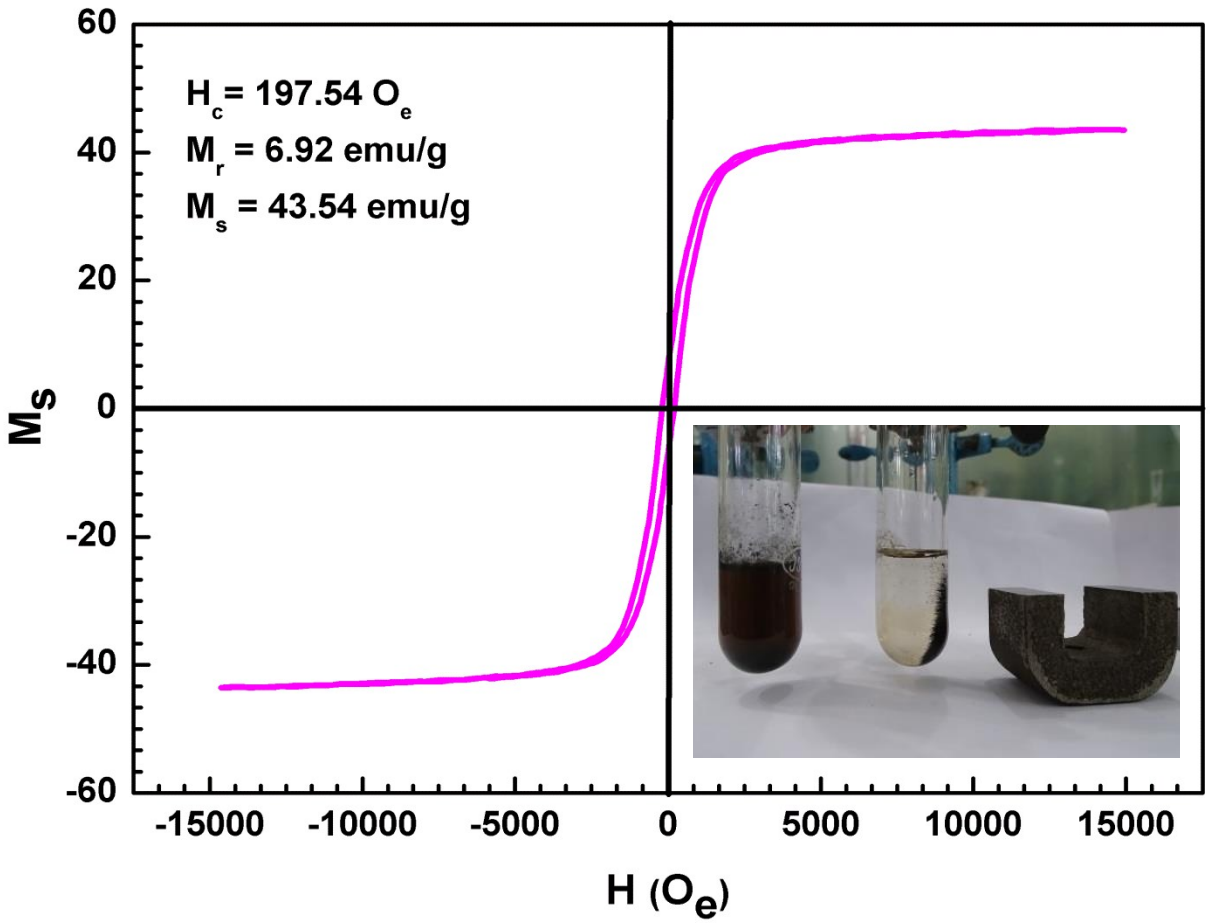

Fig. 6 Variation of magnetization (M) with magnetic field (H) at room temperature for Ni nanoparticles supported on rGO sheets

View Article Online
DOI: 10.1039/C5RA22601E

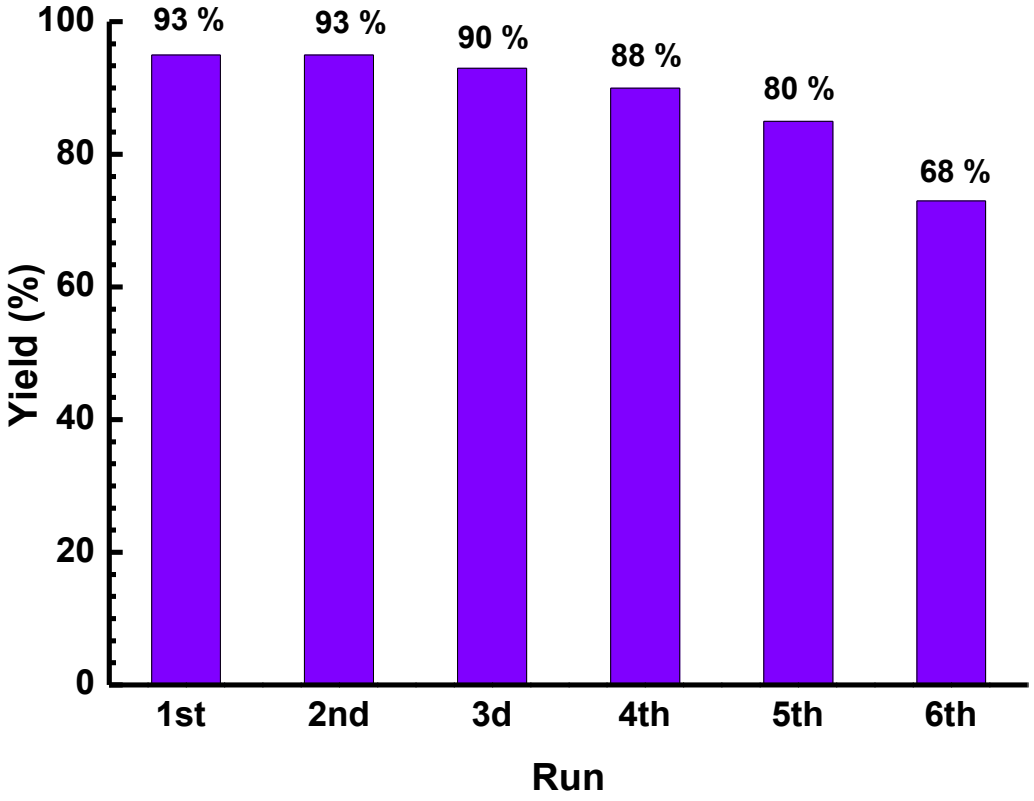

Fig. 7 Reusability of the Ni nanoparticles-rGO catalyst for the Sonogashira-cross coupling reaction

View Article Online
DOI: 10.1039/C5RA22601E

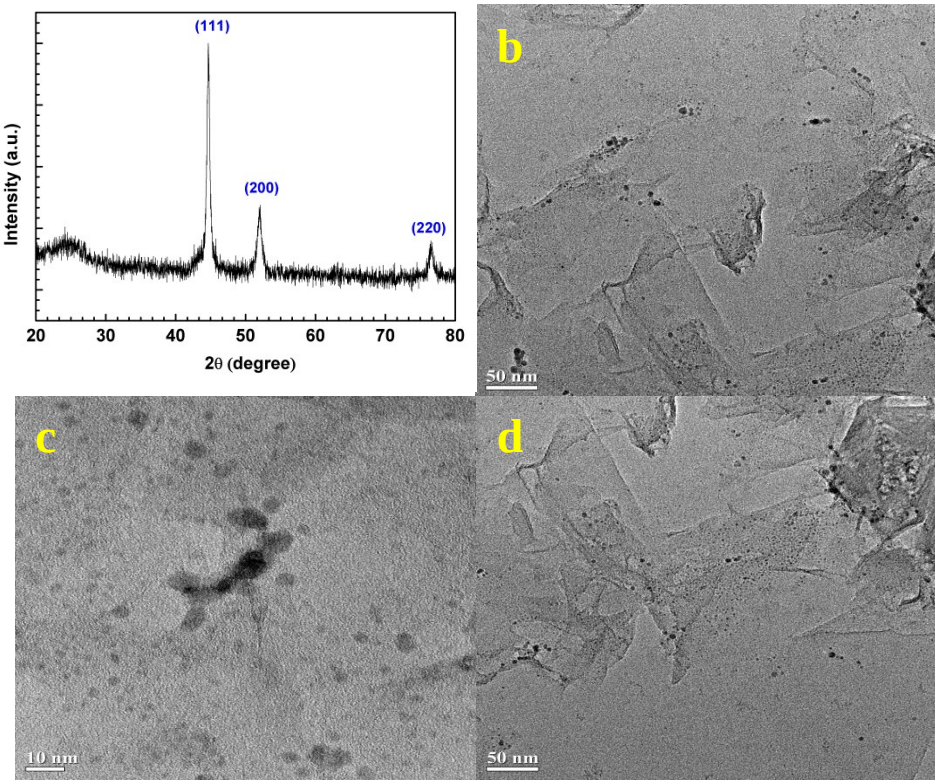

Fig. 8 Characterization of the Ni nanoparticles-rGO catalyst after performing the reaction (a) XRD pattern, (b-d) TEM images

View Article Online
DOI: 10.1039/C5RA22601E

Graphical abstract